To be published in "Applied Ocean Research".

Slow drift eddymaking damping of a ship

by

Odd M. Faltinsen, Professor, Division of Marine Hydrodynamics, Norwegian Institute of Technology, Trondheim

Bjørn Sortland, Senior Research Engineer, MARINTEK, Trondheim

ABSTRACT

This paper discusses how to obtain eddymaking damping coefficients for slow drift oscillations of a moored ship in irregular waves. By deriving a simple expression for the standard deviations of the motions it is shown that it is not necessary to have great accuracy in predicting the damping coefficients. A single vortex method has been derived and used together with experimental U-tube results to discuss the hull parameter dependence of eddymaking damping. The single vortex method is shown to agree well with experimental results for midship sections without bilge keels. The effect of a bilge keel is strong at small KC-numbers and cannot be predicted theoretically by a simple single vortex model.

NOMENCLATURE

A_{jk}	Added mass matrix
B_{jk}	Linear damping matrix due to wave drift force damping
B	Ship beam
b	Bilge keel depth
C_D	Drag coefficient based on ship draft (see equation (8))
C_M	Mass coefficient (see equation (8))
C_S	Friction factor in surge (see equation (1))
k_{jk}	Restoring matrix due to mooring. k_{j6} contain also changes in mean evironmental loads due to a rotation η_6.
D	Ship draft
F_i	Slow drift excitation force components
g	Acceleration of gravity
H_S	Significant wave height
I_{66}	Yaw mass moment of ship
KC	Keulegan-Carpenter number based on ship draft
L	Length between perpendiculars or model length
M	Ship mass
Rn	Reynolds number based on ship draft
r	Bilge radius
S_w	Average wetted ship surface
S_F	Slow drift excitation spectrum in surge. The spectrum is one-sided.
t	Time variable
U	Instantaneous free stream velocity
U_o	Amplitude of the free stream velocity
W	Width of the measuring section in the U-tube
(x,y,z)	Cartesian coordinate system (see Fig. 1)
(x,y)	Two-dimensional coordinate system (see Fig. 13)
z=x+iy	(See Fig. 13)

η_i	Slow drift rigid body motion η_1 = surge, η_2 = sway, η_6 = yaw
ρ	Mass density of water
ω	Circular frequency of oscillation
(ξ,η)	Two-dimensional auxiliary plane in the Schwartz-Christoffel transformation (see Fig. 13)
$\zeta=\xi+i\eta$	(See Fig. 13)
ν	Kinematic viscosity coefficient
$\omega_{n\bar{m}}$	Natural circular frequency in mode of motion $\bar{m}$ m = 1 surge, m = 2 sway, m = 6 yaw

INTRODUCTION

Present day theoretical methods are not accurate enough to predict slow drift oscillations of a moored ship in irregular waves. One of the weak points has been the uncertainty of deciding suitable damping coefficients. Idealistically one would like to be able to solve the Navier-Stokes equations which would avoid the need to find the damping coefficients. However this is not realistic at the high Reynolds number flows that one is interested in because of limitations in computer facilities. Also there is a need for more research and comparative studies between theory and experiments. A more realistic approach than solving Navier-Stokes equations is to use a vortex tracking method, but still we are cautious in recommending that a vortex tracking method be used in routine calculations. One needs more control over the accuracy of the predictions in order to justify the excessive computer time. Further there are problems in predicting separation points and secondary separation effects for oscillatory flow.

An alternative is to obtain damping coefficients by experimental means, but it is shown in Faltinsen, Dahle and Sortland[1] that free decay tests are not without problems. A better alternative for viscous sway and yaw damping is to use a U-tube facility to test different ship sections.

The slow drift hydrodynamic damping can be classified as damping due to skin friction, eddymaking, wave drift force and Munk moment effects. We will concentrate on eddymaking damping. When discussing the damping one should have in mind that the standard deviations of the slow drift motions are not very sensitive to inaccuracies in the damping coefficients as can be shown by deriving a simplified solution for them.

A single vortex model has been used together with U-tube results to explain the dependence of 2-D drag coefficients on geometrical hull parameters at low KC-numbers. For slow drift damping $KC < 10$ is of primary interest. The single vortex method represents the vorticity shed from a separation point by one single vortex. The time development of the vortex strength and the position is determined by a Kutta condition at the separation point and a zero-force condition on the sum of the vortex and the cut between the vortex and the separation point. A Schwartz-Christoffel transformation is used to solve the problem. Any contour shape can be considered, but the separation point has to be known and fixed. The single vortex method is shown to agree well with experimental results for midship sections without bilge keels, but the effect of bilge keel is not satisfactory predicted. The main results from the discussion of the damping coefficients are that eddymaking damping is most important for sway and yaw motions and is sensitive to free surface effects at high KC-numbers. The effect of beam/draft ratio is generally small but bilge keel dimensions and bilge radius have a significant effect. Also the scale effects are most pronounced when the flow separates from curved surfaces at high KC-numbers and three-dimensional effects should then be considered.

Even if in some cases one can obtain satisfactory estimates of the damping coefficients for slow drift oscillations of a moored ship in irregular waves, it does not necessarily mean that the prediction of the slow drift response will be satisfactory. In Faltinsen et.al. [1] it was stressed that the complete theoretical framework for slow drift oscillations need more study. The agreement between theory and experiment with a generally used calculation procedure was only partly satisfactory for the surge motion but sway motion showed better agreement.

EQUATIONS OF MOTIONS

In the following chapter the equations of motion for horizontal slow drift oscillations of a moored ship in irregular seas are formulated. This is done in order to identify the damping terms and to derive a simple result for the standard deviations of the motions which is of importance in establishing required accuracy in the estimation of the damping terms.

A cartesian coordinate system (x,y,z), is fixed in space, will be used with the origin of the coordinate system in the mean water plane and the z-axis is vertical and positive upwards. When the ship is in the mean position the z-axis passes through the vessel's centre of gravity. In the same position the x-z-plane is a symmetry plane for the ship, the x-axis is positive in the aft direction and the y-axis is positive in the starboard direction (see Fig. 1). The ship can move as a rigid body in six degrees of freedom, i.e. surge η_1, sway η_2, heave η_3, roll η_4, pitch η_5, and yaw η_6. The effect of current and wind are neglected.

The three coupled equations of slow drift motion are

Surge:

$$(M+A_{11})\frac{d^2\eta_1}{dt^2} + \frac{\rho}{2} C_s S_w \frac{d\eta_1}{dt}\left|\frac{d\eta_1}{dt}\right| + B_{11}\frac{d\eta_1}{dt} + k_{11}\eta_1 + k_{16}\eta_6 = F_1(t) \quad (1)$$

Sway:

$$(M+A_{22})\frac{d^2\eta_2}{dt^2} + k_{22}\eta_2 + A_{26}\frac{d^2\eta_6}{dt^2} + k_{26}\eta_6 + B_{22}\frac{d\eta_2}{dt} + B_{26}\frac{d\eta_6}{dt}$$

$$+ \int_L \frac{\rho}{2} C_D(x) D(x) \left|\frac{d\eta_2}{dt} + x\frac{d\eta_6}{dt}\right| \left(\frac{d\eta_2}{dt} + x\frac{d\eta_6}{dt}\right) dx = F_2(t) \quad (2)$$

yaw:

$$(I_{66}+A_{66})\frac{d^2\eta_6}{dt^2}+k_{66}\eta_6+A_{62}\frac{d^2\eta_2}{dt^2}+k_{62}\eta_2+B_{62}\frac{d\eta_2}{dt}+B_{66}\frac{d\eta_6}{dt}$$

$$-A_{22}\frac{d\eta_2}{dt}\frac{d\eta_1}{dt} \qquad (3)$$

$$+\int_L \frac{\rho}{2}C_D(x)D(x)\left|\frac{d\eta_2}{dt}+x\frac{d\eta_6}{dt}\right|\left(\frac{d\eta_2}{dt}+x\frac{d\eta_6}{dt}\right)xdx = F_6(t)$$

It should be noted that the high frequency motion due to waves is not included although this may have some relevance in the drag force term.

In the equations of motions M = mass of the ship and I_{66} = yaw mass moment of inertia. A_{jk} are the added mass coefficients based on strip theory and the "zero-frequency" assumption. The latter implies that the "rigid-wall" condition can be used on the free-surface. k_{jk} = restoring force coefficients for the mooring system which for simplicity is assumed to be linear. Changes in mean environmental loads due to a rotation η_6 are included in k_{j6}. B_{ij} = wave drift force damping coefficient.

$F_1(t)$ and $F_2(t)$ are the slow drift excitation force components along the x- and y-axis and $F_6(t)$ = slow drift excitation moment in yaw. The mean values of $F_i(t)$ are all non-zero.

In the surge velocity square viscous damping term, ρ = mass density of sea water and S_w = average wetted ship surface.

The viscous damping in sway and yaw is based on strip theory and the cross-flow principle. This, however, is questionable if the resultant incident velocity direction is close to the x-axis of the ship. In the damping term, $D(x)$ and $C_D(x)$ = local draft and drag coefficient, respectively and the integration is along the length L of the ship. In the yaw equation there is a damping term due to the Munk moment effect.

Skin friction damping is most important for surge motion especially for low sea states and it cannot be completely neglected for sway and yaw motion at low KC-number when the boundary layer flow is laminar. Faltinsen et.al.[1] have presented an example where the "wave drift force damping" in surge was 85% of the total surge damping for H_S = 8.08 m while for H_S = 2.8 m the skin friction damping was nearly 100% of the surge damping. This was for a ship 235 m long. When the boundary layer is laminar, the skin friction damping is linear.

Wave drift force damping is the most important damping contribution to surge motion in higher sea states. The reason for the sea state dependence is that the wave drift force damping is theoretically proportional to H_S^2. It is also of importance for sway and yaw motions, but the significant contribution from eddymaking damping in these modes implies that wave drift force damping has smaller relative importance in sway and yaw than in surge motion. Scale effects are not considered to be important for wave drift force damping.

The eddymaking damping is most important for sway and yaw motions but for surge motion it can often be neglected. In this context we will particularly concentrate on eddymaking damping and describe how to obtain it theoretically or by means of U-tube experiments. Before going into detail we give a simplified solution equations (1)-(3) in the frequency domain. This provides a starting point for assessing what accuracy is needed in the estimation of damping coefficients.

In order to develop a simplified solution the equations will be decoupled and Pinkster's formula[2] can then be applied to find the

standard deviation of the motions if the damping is linear. For surge motion the damping is nearly linear for high sea states. One may then write the mean square surge velocity as

$$\sigma^2_{\dot{\eta}_1} = \int_0^\infty \frac{\omega^2 S_F^{(1)}(\omega)\,d\omega}{\left\{[-\omega^2(M+A_{11})+k_{11}]^2 + [\omega B_{11}]^2\right\}} \tag{4}$$

Here $S_F^{(1)}$ is the slow drift excitation spectrum in surge. When the damping is small the integral may be approximated by the white noise formula, to yield

$$\sigma_{\dot{\eta}_1} = \omega_{n1}\left[\frac{\pi S_F^{(1)}(\omega_{n1})}{4k_{11}B_{11}}\right]^{1/2} \tag{5}$$

where ω_{n1} = natural circular frequency in surge. Equation (5) implies, for instance, that a 100% increase in the damping B_{11} results in a 29% reduction in r.m.s. response. Since $S_F^{(1)}$ is proportional to H_s^4 and B_{11} is proportional to H_s^2, equation (5) implies also that the standard deviation of slow drift surge motion is proportional to H_s.

In sway motion it will be assumed that the major damping contribution is due to nonlinear viscous effects. In order to apply Pinkster's formula one must linearize the damping term by an equivalent linearization technique. By assuming that the response is Gaussian distributed the equivalent linear damping term is given by the Borgman linearisation

$$B_{22} = \left[\frac{\rho}{2}\int_L dx C_D(x) D(x)\right]\sqrt{\frac{8}{\pi}}\,\sigma_{\dot{\eta}_2} \tag{6}$$

The Gaussian assumption is an approximation but it has some

justification for a lightly damped randomly excited system. Jensen[3] used the experimental results from Faltinsen et.al's study and showed that the Gaussian assumption is an appropriate approximation. If one also approximates the integral for the standard deviation in sway in a similar way to surge, we have

$$\sigma_{\dot{\eta}_2} = \left[\frac{\pi S_F^{(2)}(\omega_{n2})}{\sqrt{\frac{32}{\pi}}\, \rho \int_L dx C_D(x) D(x) \quad (M+A_{22})} \right]^{1/3} \tag{7}$$

Here $S_F^{(2)}(\omega_{n2})$ = slow drift excitation spectra in sway at the natural sway frequency. Equation (7) shows that the standard deviation in sway is proportional to $H_s^{4/3}$. Further it is evident that the sway motion is even less sensitive to the damping than the surge motion. A 100% increase in the damping means a 20% reduction in the r.m.s. response. This is important to know when the damping coefficients are discussed in the following chapters.

EXPERIMENTAL AND THEORETICAL DETERMINATION OF EDDYMAKING DAMPING COEFFICIENTS

The theoretical procedure that was followed to determine the two-dimensional drag coefficients in sway and yaw eddymaking damping is outlined in Appendix A. It is based on a single vortex model, applicable for small KC-numbers and the separation points have to be known and fixed. Due to the method's simplicity it provides a practical means to calculate different test cases easily. This will be done in the next section. In order to assess the method's accuracy, the results will be compared with experimental results by Bearman et.al.[4] without free surface effects and with experimental results obtained in the U-tube facility at the Marine Technology Centre in Trondheim. The dimensions of the U-tube are given in Fig. 2. The natural period of oscillation of the fluid motion is 2.86 sec. In the experiments the free surface was simulated by placing the ship section upside down on a false bottom in the U-tube (see Fig. 3). This is legitimate from a wave generation point of view because the slowly varying ship motions generate no waves and the free surface acts as a rigid wall.

The boundary condition on the free surface is a no-shear condition, but on a wall there is a no-slip condition. As long as the flow does not separate either at the wall in the model tests or at the free surface in reality, the difference in the boundary condition is not considered to be a serious drawback. No separation was observed at the wall in the model tests, but it was difficult to make observations in the vicinity of the ship sections. The boundary layer thickness was estimated to be about 3 mm which is small in comparison to the height of the model.

The ship section is extending from one side window to the other. To prevent any effect of the side walls a dummy section is placed on either side of the measuring section, see Fig. 4. The gap between the dummy and the measuring section is adjusted to be 0.1 mm and therefore is not believed to have any effect on the flow around the test section.

The forces on the measuring section are measured by force transducers using strain gauges. The force transducers are supported outside the tank and enter into the measuring section through holes in the side windows and dummy sections.

Using a false bottom it is possible to look into the tank along the bottom, which is needed when doing flow visualization. No water should be able to pass under the test section and to achieve this the test section should be lying flat on the bottom. On the other hand this will give a friction force between the measuring section and the bottom, which has to be avoided. By letting the measuring section have almost no weight in water and placing it on a limited number of small round polystyrene particles with a diameter of about 0.5 mm, this friction has been minimized. The static friction force for the measuring section in this condition have been found to be less than 0.01 N which should be compared to the lowest measured dragforce of 0.35 N. The section was also installed without such particles and with a gap between the bottom and the section of about 0.2 mm. In this condition no friction forces were acting between the bottom and the measuring section.

In order to evaluate the importance of water oscillating in the gap between the ship section and the wall a theoretical analysis based on laminar boundary layer flow is outlined in Appendix B. According to the theory the maximum velocity is ~ 0.12

times the maximum free stream velocity U_o when the test sections are mounted with a gap of 0.5 mm. For a gap height of 0.2 mm the maximum velocity is reduced to $0.02\ U_o$. Flow visualizations showed a qualitative agreement with the estimates. The resulting frictional force on the test section is estimated theoretically to be less than 0.5% of the dragforce as follows. At the entrances to the gap flow separation will occur. If we base an estimate of the shed vorticity per unit time $\frac{\partial \Gamma}{\partial t}$ on the maximum theoretically estimated gap velocity, we find $\frac{\partial \Gamma}{\partial t}$ to be $0.007\ U_o^2$ for a gap heigth of 0.5 mm. Flow visualizations showed vortex shedding at the entrances, but based on the estimates of $\frac{\partial \Gamma}{\partial t}$ it is likely to have no important effect on the dragforces.

In the experiments a gap height of 0.5 mm was used for the ship without bilge keels. The ship section with bilge keels was run with a gap height of 0.2 mm and no polysterene particles. For KC-number greater than 10 the section was rotating and hitting the bottom, but for small KC-numbers the section was not moving at all, and the friction force between the section and the bottom was zero.

Force measurements have been performed on the midship section of the ship studied in ref.[1,5,6] The dimensions of the measuring section are given in Fig. 5. The beam-draft ratio of this section is 2.7 and the ratio between the bilge radius and draft is 0.22. When the section is placed on the false bottom, it has a blockage ratio of 0.14. The section is made of plexi-glass and polished to a very smooth surface. The effect of bilge keel was also tested. The bilge keel depth to draft ratio were 0.03 and 0.06 and they were fitted normal to the bilge surface at $\beta = \pi/4$ (see Fig. 5). The ends of the bilge keels were sharp corners with a negligible interior angle.

The calibration factors for the force transducers are found from 7 different calibration sequences achieved by use of a special weight giving a horizontal force (drag direction). Plots of the input and calculated forces for each of the two force transducers showed no hysteresis and both seemed to be linear. The difference between the input and calculated total force for all 7 calibrations has a maximum of 0.01 N and a standard deviation of 0.005 N which demonstrates the repeatability of the force measuring system. For the lowest KC-number used, the total in-line force on the cylinder is about 0.35 N giving a minimum signal to noise ratio of 70 relative to this standard deviation.

Placing weights on the top of the model gave unwanted horizontal force readings. The strain gauges force transducers used were found to give a false force reading in horizontal direction when they were loaded in vertical direction and vice versa. This phenomena is called crosstalk and gives an over-estimation of the horizontal forces introduced by the lift forces on the section. The increase of the measured horizontal force is not corrected for, but estimated to be about 3%.

The results are presented as drag and mass coefficients C_D and C_M as defined by Morison's equation, which states that the in-line force can be written as

$$F = \rho \, BDL \, C_M \, \dot{u} + \frac{\rho}{2} \, DL \, C_D \, u|u| \qquad (8)$$

Here u = instantaneous free stream velocity, L,B and D = length, beam and draft of the test section, and C_M, C_D have been calculated from a Fourier analyses of the measured forces on the test section.

A PARAMETRIC STUDY OF EDDYMAKING DAMPING

The following discussion is based on a strip theory approach which means that two-dimensional cross-sections will be studied, focussing on midship sections. The drag coefficients depend on free-surface effects, beam-draft ratio, bilge keel dimensions, bilge radius, current, Reynolds number, roughness ratio and Keulegan-Carpenter number (KC). Some of these effects will be discussed below. A simple single vortex model (see Appendix A) and U-tube results will be used to explain the results.

Free surface effects

The free surface acts similar to an infinitely long splitter plate. Hoerner[7] gives C_D-values for bodies with splitter plates of finite length in steady incident flow (KC = ∞). The splitter plate shows clearly a lowering effect on the drag coefficient.

A simple explanation of why there is a lowering effect of the free surface on the drag coefficient for KC = ∞ can be given by means of Fig. 6. The shed vorticity is represented by one single vortex of strength Γ, which is a function of time. To account for the free surface effect one has to introduce an image vortex which ensures zero normal velocity on the free surface. The image vortex introduces a forward motion effect on the real vortex and as time goes on this forward motion effect becomes so strong, that the total velocity of the real vortex goes to zero. The consequence of a decaying vortex velocity is that the drag coefficient goes to zero. In reality the vorticity is distributed in space and will have different convection velocities, but the numerical results by Aarsnes[5] (which is based on Faltinsen and Pettersen's[8] thin shear layer model) show a decaying effect of the drag coefficient with time for ship cross-sections in a current. In reality the drag coefficient will not go to

zero since three-dimensional effects and diffusion will affect our idealized physical picture. If the splitter plate were not there, instabilities would cause a Karman vortex street to develop behind the double body and the vorticity would then be convected away, resulting in a higher drag coefficient.

When the KC-number is low, the eddies will stay symmetric for the double body without splitter plate. This means the free surface has small effect for low KC-numbers.

Beam-draft ratio effects

Experimental results by Tanaka, Ikeda and Nishino [9] show the height-length ratio has a small effect on the drag coefficient for two-dimensional cross-sections of rectangular forms. One exception was for small height-length ratios at the lowest tested KC-number 10. If one translates the results to midship cross-sections, it implies that the beam-draft ratio B/D has little influence on the drag coefficient when $B/2D > 0.4$.

The single vortex method will be used to discuss the effect of beam-draft ratio at low KC-number. The results for rectangular cross-sections are presented in Fig. 7 for $KC = 2$. As excepted from Graham's local analysis [10], it is seen that the results for rectangular cross-sections are nearly independent of the KC-number for small KC-numbers. It is evident from Fig. 7 that there is no significant variation over a wide range of B/D values from 0.2 to 10. These results are in conflict with the experimental results by Tanaka et.al. for the lowest beam-draft ratios but the reason may be the difference in KC-number. The absolute value of the drag coefficient is surprisingly close to the experimental value by Bearman et.al. [4] for a square section

at low KC-numbers. Due to the simplicity of the method used, one should be careful when drawing conclusions about the accuracy of the single vortex method: What one can hope for is that the single vortex method predicts the correct trends in a qualitative sense.

Bilge keel effects

Results by the single vortex method are presented in Fig. 8 for the cross-section shown in Fig. 5 fitted with bilge keels. There is a strong effect of the bilge keel depth, in particular for the smaller KC-numbers. The C_D-value is increasing nearly linearly with the bilge keel depth.

Experimental U-tube results for C_M and C_D are presented in Fig. 9 and 10 as a function of KC for two different bilge keel depths. The experimental C_M-value for small KC-numbers is in reasonable agreement with the theoretical values obtained by the procedure in Appendix A. The theoretical value neglects the influence of shed vorticity and friction and becomes more correct as $KC \to 0$. Friction is estimated to increase the experimental C_M-value by 0.02. The experimental C_M-value should be reduced about 4% because of friction and crosstalk before it is compared to the theoretical value. One should also keep in mind that the theoretical value is not exact, but depend upon numerical approximations.

The theoretical C_D-values obtained by the single vortex method do not agree very well with the experimental C_D-values. A small fraction of the difference can be explained by friction forces; According to the procedure in Appendix A this will result in a C_D of $0.5/KC$ for the Reynolds numbers used in the experiments. One reason for the low theoretical C_D-values

may be that it is only possible to examine theoretically the first half cycle of oscillation. It is likely that the shed vorticity in later oscillation cycles get stronger which will increase the C_D-values. It should also be realized that the bilge keel depth is of the order of magnitude of the boundary layer thickness, but theoretically it is assumed that the bilge keel depth is large compared to the boundary layer thickness.

Bilge radius effects

Experimental results by Tanaka et.al.[9] for $KC \geq 10$ show a strong effect of the bilge radius on the drag coefficient such that increasing the bilge radius decreases the drag coefficients. Results by the single vortex method with a finite bilge keel depth show the same tendency (see Fig. 11).

Experimental U-tube results without bilge keels are presented in Figs. 9 and 12 for the test section presented in Fig. 5. The theoretical C_D-values obtained by the single vortex method is in reasonable agreement with the experimental values. These theoretical values were calculated with a small finite bilge keels of dimensions $b/D = 0.02$ mounted at a bilge angle $\beta = \pi/4$ (see Fig. 5). The results show sensitivity to KC-number where there is a tendency for the drag coefficients to decrease with decreasing KC-number. This is expected from Graham's local analyses[10] and from known experimental results for circular cylinders at low Keulegan-Carpenter numbers.

In Fig. 12 our experimental results are compared with experimental values by Bearman et.al. for a rectangular cross section and show a strong decay of C_D with bilge radius at small KC-number. This cannot be due to the small difference in beam-draft

ratio between Bearman et.al's and our test section. For larger KC-number this decay is not so strong as also shown by Tanaka et.al. who only examined KC $\geq$ 10.

Effect of laminar or turbulent flow

The classical results for a circular cylinder show that there is a critical Reynolds number below which the boundary layer is laminar. In the supercritical and transcritical range the boundary layer is turbulent. The consequence of this is that the separation points are quite different in the subcritical and transcritical Reynolds number range resulting in a difference in drag coefficients. Thus for marine structures one often has the situation that model tests have to be performed in the subcritical range, while the full scale situation is in the transcritical range. However, when the separation occurs from sharp corners one would not expect any severe scale effects.

Aarsnes et.al.[6] have shown that the drag coefficient may be substantially different depending on laminar or turbulent separation. This is also evident from Delaney and Sorensen's results.[11] All these results are for KC = ∞ , i.e. steady incident flow. Aarsnes et.al's results were for ship cross-sectional forms without bilge keels. The reason to the difference in subcritical and transcritical flow is that the flow separates more easily in subcritical flow which is laminar and the flow separates at the "leading" bilge. However a turbulent boundary layer which occurs in transcritical flow can sustain a larger adverse pressure gradient without separating. This is the reason why there is no separation at the "leading" bilge for transcritical

flow. If separation occurs simultaneously at both corners the drag coefficient is roughly speaking twice the value of that when separation occurs at only one corner at a time.

At small KC-numbers the separation occurs at both bilges for the midship cross-section and therefore the scale effect on the drag coefficient is not expected to be severe. In any case one should have in mind the introductory remark that a 100% increase in drag coefficient will not cause more than 20% reduction in the standard deviation of the motions. In order to get an estimate of what the scale effect may be, the single vortex method has been applied with two different sets of positions for the separation points. The first case with $\beta = \pi/4$ has been discussed already (see Fig. 5). In the other case $\beta = \pi/8$. The separation points at the two bilges were symmetric with respect to the center plane. The results, presented in Table 1, show some sensitivity to the separation point position. This discussion of the effect of laminar or turbulent flow is simplistic. More experimental results are needed to support the conclusions.

Three-dimensional effects

Aarsnes et.al.[6] point out that three-dimensional effects at the ship ends will reduce the dragforce relative to a pure strip-theory approach. One way of taking this into account would be to use a reduced effective incident flow at the ship ends as predicted in a qualitative way by Aarsnes et.al. Physically the reduced inflow is due to the eddies at the ship ends and this can be translated into a three-dimensional reduction factor of the two-dimensional drag coefficients. The effect is strong at the ship ends and in total will amount to approximately 20% reduction in the sway damping. The effect on yaw will be larger.

CONCLUSIONS

It is shown that the standard deviations of slow drift motions are not sensitive to moderate changes in the damping coefficients. The eddymaking damping coefficients are discussed and it is shown by a single vortex method and U-tube experiments that bilge keel dimensions and bilge radius may have a significant effect on the eddymaking damping. The single vortex method agrees well with experimental results for midship sections without bilge keels but cannot explain the effect of bilge keels.

ACKNOWLEDGEMENT

The work is part of the research project "Marine structures", which is financially supported by The Royal Norwegian Council for Scientific and Industrial Research, (NTNF), Statoil, Norsk Hydro, Det norske Veritas and Norwegian Institute of Technology,

REFERENCES

1 Faltinsen, O.M., Dahle, L.A. and Sortland, B. Slowdrift damping and response of a moored ship in irregular waves, Proceedings of 3rd OMAE Conference, Tokyo, April 1986.

2 Pinkster, S.A. Low frequency phenomena associated with vessels moored at sea, Paper SPE 4837, 1974, European Spring Meeting at SPE-AIME, Amsterdam.

3 Jensen, R. Master thesis, Division of Marine Hydrodynamics, Norwegian Institute of Technology, 1985.

4 Bearman, P.W. et.al. Forces on cylinders in viscous oscillatory flow at low Keulegan-Carpenter numbers, Journal of Fluid Mechanics, May 1985.

5 Aarsnes, J.V. Current forces on ships, Dr.ing.thesis, Report UR-84-39, Department of Marine Technology, The Norwegian Institute of Technology, 1984.

6 Aarsnes, J.V., Faltinsen, O. and Pettersen, B. Application of a vortex tracking method to current forces on ships, Proceedings of Separated Flow around Marine Structures, Norwegian Institute of Technology, June 1985.

7 Hoerner, S.F. Fluid dynamic drag, Published by the author, 1965.

8 Faltinsen, O. and Pettersen, B. Vortex shedding around two-dimensional bodies at high Reynolds number, Proceeding of 14. Symp. on Naval Hydrodynamics, The University of Michigan Ann Arbor, 1982.

9 Tanaka, N., Ikeda, Y. and Nishino, K. Hydrodynamic viscous force acting on oscillating cylinders with various shapes, Proceedings of the 6th Symposium of Marine Technology, The Society of Naval Architects of Japan, Dec. 1982.

10 Graham, J.M.R. The forces on sharp-edged cylinders in oscillatory flow at low Keulegan-Carpenter numbers, J. Fluid Mech. 97, 331-346, 1980.

11 Delaney, N.K. and Sorensen, N.E. Low-speed drag of cylinders of various shapes, NACA Technical Note 3038, 1953.

12 Brown, C.E. and Michael, W.H. 1955 Nat. Adv. Comm. Aero Tech. Note 3430.

13 Davis, R.T. Numerical methods for coordinate generation based on a mapping technique, VKI LS 81-5, Comp. Fluid Dynamics, 1981.

14 Graham, J.M.R. Vortex shedding from sharp edges, I.C. Aero Report 77-06, Nov. 1977, Department of Aeronautics, Imperial College of Science and Technology, London.

15 Graham, J.M.R. Forces on cylindrical bodies in oscillatory flow at low Keulegan-Carpenter numbers, Mechanics of Wave-induced Forces on Cylinders (editor T.L. Shaw), Pitman Publishing Limited, 1979.

16 Schlicting, H. Boundary layer theory, Mc Graw-Hill Book Company, Seventh Edition, 1979.

17 Landau, L.D. and Lifschitz, E.M. Fluid mechanics, Pergamon Press, 1959.

APPENDIX A

SINGLE VORTEX MODEL

A single vortex model will be used to analyse vortex shedding around ship cross-sections at low KC-number and the separation points will be fixed. The approach is significantly simpler than for instance the vortex tracking method by Faltinsen and Pettersen [8] or any solver of the Navier-Stokes equations.

The motivation for choosing a simple approach is to be able to discuss the sensitivity of the drag coefficient to changes in geometrical parameters. A simple model is also needed in order to derive a practical and realistic model for the wave drift force damping in sway and yaw that accounts for the interaction between first order wave induced motions and the vortex shedding.

The body and the coordinate system are defined in Fig. 13. The free surface is represented by a rigid wall. The flow is oscillating harmonically with small amplitudes of motion which causes the flow to separate from two fixed points z_i^s on the body. Each shed vortex sheet will be represented by a point vortex $\Gamma_i(t)$ at a position $z_i(t)$. Since each point vortex represents a vortex sheet attached to a separation point z_i^s, it must be joined to z_i^s by a cut representing the sheet. This simplified model was first suggested by Brown and Michael [12] to represent the spiral vortex above the leading edge of a slender wing.

Since the point vortices are shed from the separation points, infinite velocities must be eliminated at the points. This implies one has to specify a Kutta condition requiring zero velocity at the separation points. A condition that requires zero

force on the sum of each vortex and its cut, is required to complete the specification of the vortex strength and its path. The zero force condition for each vortex can be written mathematically as

$$\frac{\partial}{\partial t}\left(\Gamma_k(z_k - z_k^s)\right) = \Gamma_k \overline{\left(\frac{d\phi}{dz} - \frac{i\Gamma_k}{2\pi(z-z_k)}\right)}\Bigg|_{z\to z_k} \qquad (9)$$

$$k = 1,2$$

Here ϕ is the complex potential in the fluid. In order to find an expression for ϕ a Schwartz-Christoffel transformation will be used. In the case of sharp corners, this can be written as

$$\frac{dz}{d\zeta} = M \prod_{i=1}^{n} (\zeta - a_i)^{\alpha_i/\pi} \qquad (10)$$

The quantity n relates to the number of corners. M is a complex constant and a_i are real constants to be determined. The angles α_i identifying the different corners, are shown in Fig. 13 measured positive in the counter clockwise direction. Davis [13] has generalized Schwartz-Christoffel transformation to curved surfaces. He has also set up a practical procedure to determine the unknowns a_i, M and this computational procedure has been followed.

The Schwartz-Christoffel transformation that was chosen, will map the lower half of the ζ plane into the fluid domain. The complex velocity potential w can now be written as

$$\phi = MU\,\zeta + i \sum_{j=1}^{2} \frac{\Gamma_j}{2\pi} \{\mathrm{Log}(\zeta - \zeta_j) - \mathrm{Log}(\zeta - \bar{\zeta}_j)\} \qquad (11)$$

Here ζ_j is the position of the vortices in the auxiallary plane ζ and U is the free stream velocity at infinity. The

branch cuts of the log-functions in (11) have to be selected so that $\phi \to U\, z$ when $|z| \to \infty$ in all directions of the fluid domain.

The Kutta condition can now be written mathematically as

$$\frac{i}{2\pi} \sum_{j=1}^{2} \Gamma_j \left[\frac{1}{\zeta_k^s - \zeta_j} - \frac{1}{\zeta_k^s - \bar{\zeta}_j} \right] = -U\, M \tag{12}$$

Here ζ_k^s is the ζ-coordinate of the separation point z_k^s.

The Brown-Michael equation (9) can be written as

$$\frac{\partial}{\partial t} \left(\Gamma_k (z_k - z_k^s) \right) = \Gamma_k \left[MU + i \sum_{j=1}^{2} \frac{\Gamma_j}{2\pi} \left\{ \frac{1-\delta_{kj}}{\zeta_k - \zeta_j} - \frac{1}{\zeta_k - \bar{\zeta}_j} \right\} \right] \frac{d\zeta}{dz}$$

$$- i \frac{\Gamma_k}{4\pi} \frac{\dfrac{d^2 z}{d\zeta^2}}{\left(\dfrac{dz}{d\zeta}\right)^2} \Bigg|_{z=z_k} \tag{13}$$

In order to start the solution, a local solution was used as the initial condition as described by Graham.[14] The horizontal force on the body can be written as

$$F_x = \int_S p\, dy \tag{14}$$

where the integration is over the wetted body surface S and

$$p = -\rho \frac{\partial}{\partial t} \mathrm{Re}(\phi) - \frac{\rho}{2} \left| \frac{d\phi}{dz} \right|^2 \tag{15}$$

Graham [14] has applied the single vortex method to different local corner flows. His results show (see Fig. 14) that the single vortex method was not significantly in error with experimental results for low KC-number if one chooses the time dependence of the undisturbed flow to be

$$U = U_o \sin \omega t \tag{16}$$

and start the solution at $t = 0$. The solution with the single vortex method can only be valid until the point when $\frac{\partial \Gamma_i}{\partial t} = 0$, but this is sufficient time for the maximum in the force due to the vortices to occur.

Numerical solution procedure

The Kutta condition was approximated as

$$\frac{\Gamma_j \sin\theta}{\pi r} = MU \tag{17}$$

where

$$\zeta_j - \zeta_j^s = r\, e^{i\theta} \tag{18}$$

From the Brown and Michael solution [12] one knows

$$\Gamma_j (z_j - z_j^s) = A_j(t) \tag{19}$$

Equation (17) and (19) were solved iteratively at each time step by first setting Γ_j equal to Γ_j from the previous time step. From equation (19) one can then determine $z_j - z_j^s$ and the corresponding ζ_j value is determined for the Schwartz-Christoffel transformation which has also to be done iteratively. When ζ_j is found one can use (17) to determine a new value of Γ_j. The procedure is now repeated until the guessed and estimated Γ_j value coincides. We have not tried to optimize the solution procedure because the CPU time is no problem. The vortex force is found by neglecting the quadratic velocity term in the Bernoulli's equation and using only the vortex part of the velocity potential. The additional term $MU\zeta$ gives the hydrodynamic mass force.

In the results presented in the main text, C_D is defined

from the maximum of the vortex force. It is non-dimensionalized with respect to the maximum velocity. The maximum vortex force does not always occur at the time of maximum velocity. For the curved surfaces, straight line segments were used to approximate the curved parts. Four elements were used on each bilge. The time stepping of the Brown and Michael equation was done by the Euler mentod.

Calculation of C_M and skin friction forces

The calculation of the mass coefficient C_M and the skin friction forces is based on non-separated flow. The boundary layer is assumed to be laminar and the Stokes solution will be used to estimate the frictional force. This results in a frictional force that is $\pi/4$ and of phase with the instantaneous velocity. The frictional contribution to C_M will be examined separately.

Based on (11) we can write the velocity potential for non-separated flow as $\mathrm{Re}(M\zeta)U$. The corresponding horizontal force on the body can be obtained by properly integrating the pressure (see equation (15)). By using the definition of C_M it follows that

$$C_M = \frac{1}{BD} \int_C \mathrm{Re}(M\zeta)\, dy \qquad (20)$$

The integration is along the wetted body surface C.

The drag force due to skin friction follows from the solution of Stokes second problem (Schlicting[16]). The tangential velocities outside the boundary layer needed in the shear force calculation follow by differentiating the complex potential $M\zeta U$ for non-

separated flow. This means the frictional drag force can be written

$$C_D = 2\sqrt{\frac{\pi}{KC\ R_n}}\ \frac{1}{D}\int_C dx\ \left|M\ \frac{d\zeta}{dz}\right| \tag{21}$$

Here $R_n = \frac{U_o D}{\nu}$, where ν = kinematic viscosity coefficient. The contribution of skin friction to C_M can be written as

$$C_M = \left(\frac{C_D D}{4\pi B}\right) KC \tag{22}$$

with C_D given by (21). This follows from using the definitions of C_M and C_D as well as using the fact that the frictional force is $\pi/4$ out of phase with the instantaneous velocity.

APPENDIX B

Theoretical investigation of the flow between the tank bottom and the ship section

The flow situation and coordinate system is shown in Fig. 15. Laminar flow will be assumed and a solution that is valid away from the entrances will be examined. The Navier-Stokes equation can be written as

$$\frac{\partial u}{\partial t} = -\frac{1}{\rho}\frac{\partial p}{\partial x} + \nu\nabla^2 u \qquad (22)$$

where u is the horizontal velocity and p is the pressure. By requiring u to be zero at the tank wall and the ship section we can write (see Landau and Lifschitz[17])

$$u = \frac{ia}{\omega} e^{-i\omega t}\left[1 - \frac{\cos ky}{\cos \frac{1}{2} kh}\right]$$

where

$$-\frac{1}{\rho}\frac{\partial p}{\partial x} = a\, e^{-i\omega t}$$

$$k = (1 + i)/\delta$$

$$\delta = \sqrt{2\nu/\omega}$$

Maximum velocity occurs at $y = 0$. The frictional force per unit area on the ship section can be written as

$$\sigma_x = -\mu \frac{ia}{\omega} e^{-i\omega t} k \cdot \tan\left(\frac{kh}{2}\right)$$

Here $\mu = \nu\rho$ is the coefficient of viscosity.
The distance h is assumed to be much smaller than the boundary layer thickness outside the gap. We may then use the pressure outside the boundary layer, i.e. the potential flow solution. We will neglect the influence of separated flow and use the

solution in Appendix A. This means

$$\frac{1}{\rho}\frac{\partial p}{\partial x} = \frac{2M}{B} i\omega U_o e^{-i\omega t}$$

where B is sectional beam. We can then write the friction force on the bottom of the ship section as

$$F_x = -2M\mu \frac{(1+i)}{\sqrt{2\nu/\omega}} \tan\left[\frac{(1+i)h}{2\sqrt{2\nu/\omega}}\right] U_o e^{-i\omega t}$$

It is the real part which has physical meaning. The drag force is associated with the term in phase with $\cos\omega t$. This means

$$C_D = \mathrm{Re}\left\{-4\frac{M}{D}(1+i)\sqrt{\frac{\pi}{KC\cdot R_n}}\cdot\tan\left[(1+i)\frac{h}{2D}\sqrt{\pi\frac{R_n}{KC}}\right]\right.$$

In a similar way one can estimate the contribution to C_M by evaluating the force contribution in phase with the acceleration.

FIGURE CAPTIONS

Figure 1 Coordinate system.

Figure 2 Main dimensions of the U-tube water tank. The tank cross section is 400 mm square inside. It is made of 8 mm water resistant aluminium alloy, with three 20 mm thick plexiglass windows in the working section and one in the right upright arm.

Figure 3 U-tube water tank with midship section mounted upside down at the false bottom.

Figure 4 Ship section mounted in the U-tube, seen from above. The section is lying upside down on the false bottom.

Figure 5 Midship section used in the U-tube. The same section has been used with and without bilge keels. Length of the measuring section is 200 mm.

Figure 6 Simple vortex system, illustrating the free surface effect.

Figure 7 Effect of beam-draft ratio on C_D.

Figure 8 Effect of bilge keel depth on C_D.

Figure 9 Experimental C_M-values for a midship section with and without bilge keels.

Figure 10 Experimental C_D-values for a midship section fitted with bilge keels.

Figure 11 Effect of bilge radius on C_D.

Figure 12 Experimental and theoretical C_D-values for a midship section without bilge keels.

Figure 13 Physical and auxiliary plane used in the Schwartz-Christoffel transformation.

Figure 14 Non-dimensional vortex force for a flat plate at low KC-number (Graham [15]).

Figure 15 Flow situation between ship section and tank wall.

TABLE CAPTIONS

Table 1 Influence of separation point.

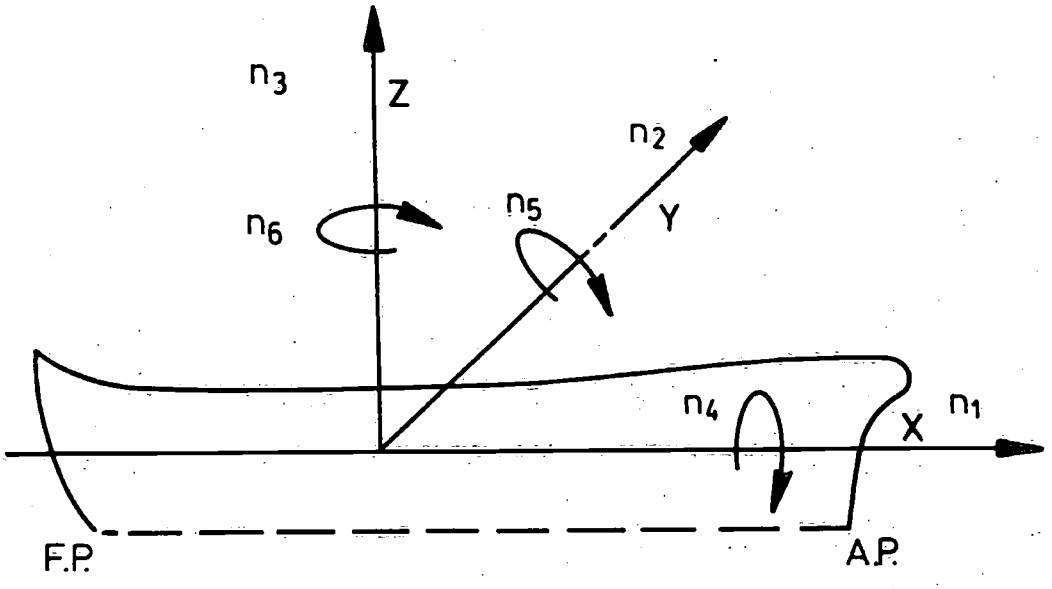

Figure 1

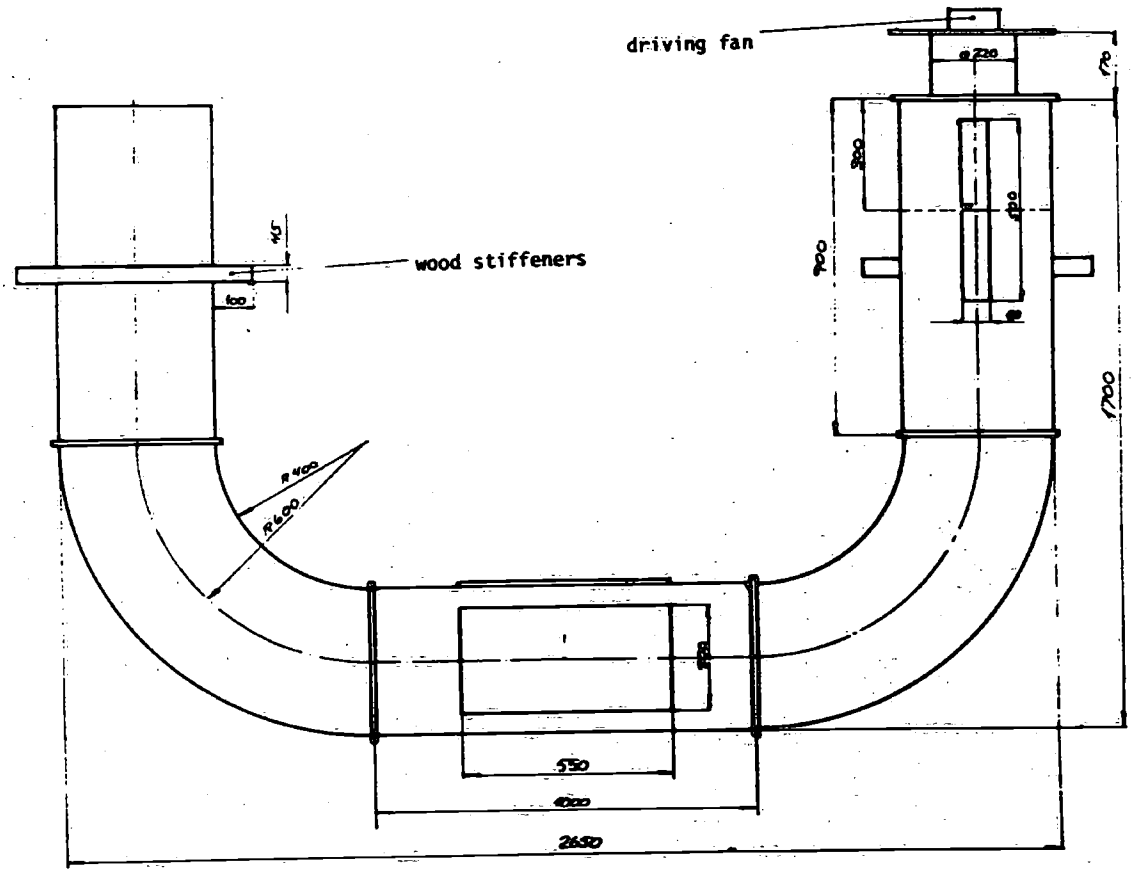
driving fan
wood stiffeners
45
100
R400
R600
300
700
1700
550
4000
2650

Figure 2

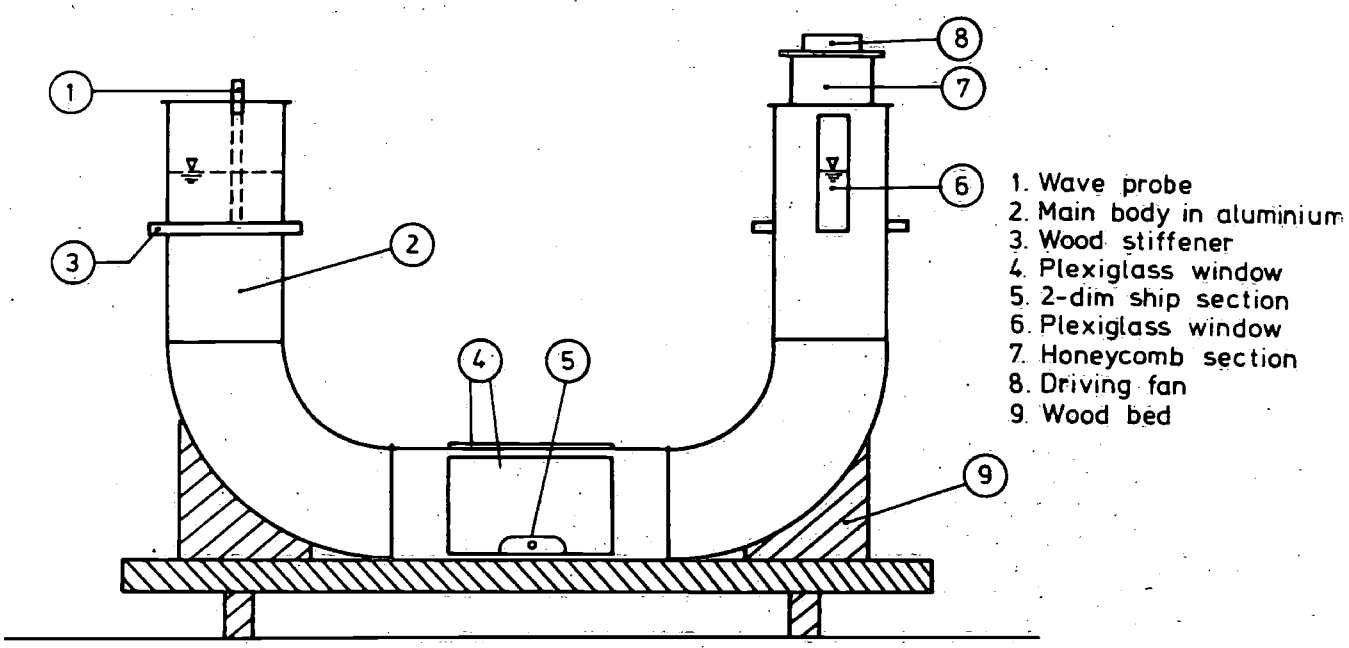
1. Wave probe
2. Main body in aluminium
3. Wood stiffener
4. Plexiglass window
5. 2-dim ship section
6. Plexiglass window
7. Honeycomb section
8. Driving fan
9. Wood bed

Figure 3

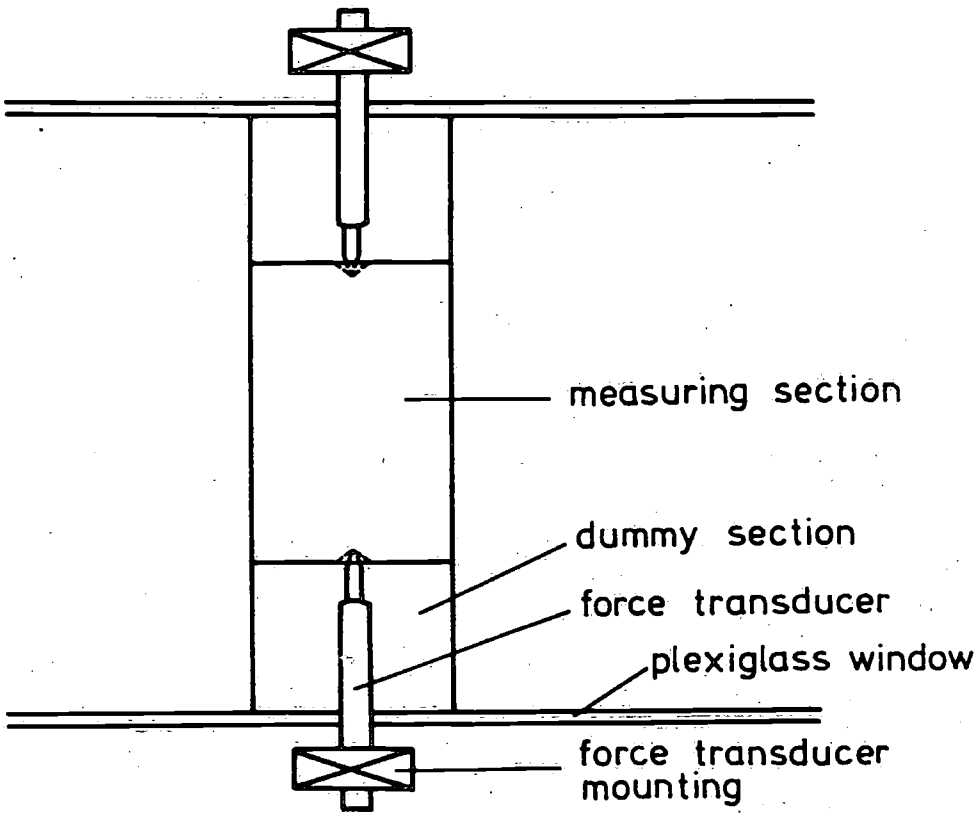
measuring section
dummy section
force transducer
plexiglass window
force transducer
mounting

Figure 4

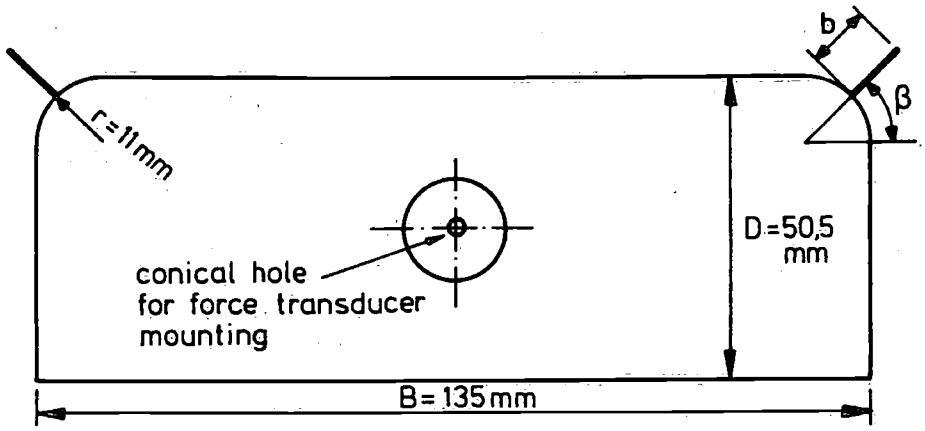
b
β
r=11mm
conical hole
for force transducer
mounting
D=50,5
mm
B=135mm

Figure 5

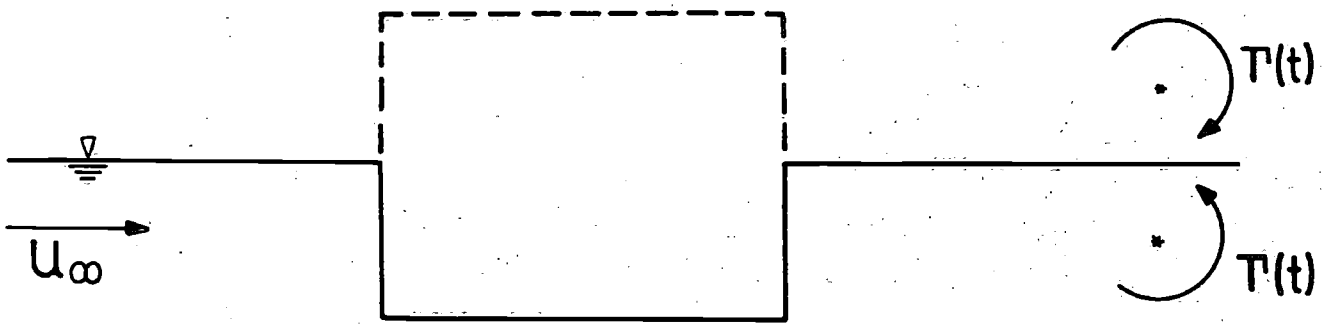

Figure 6

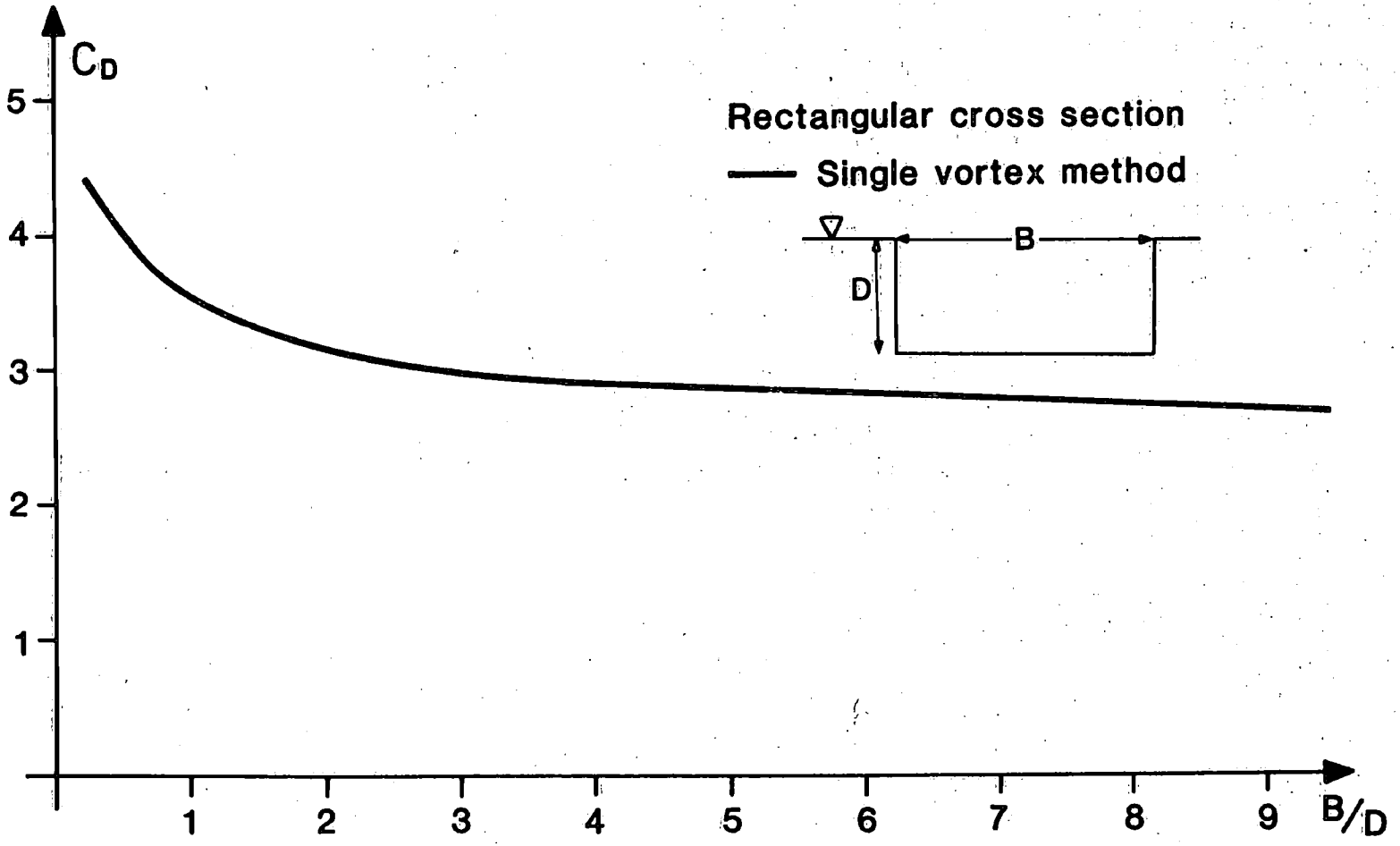
C_D
5
4
3
2
1
Rectangular cross section
Single vortex method
B
D
1
2
3
4
5
6
7
8
9
B/D

Figure 7

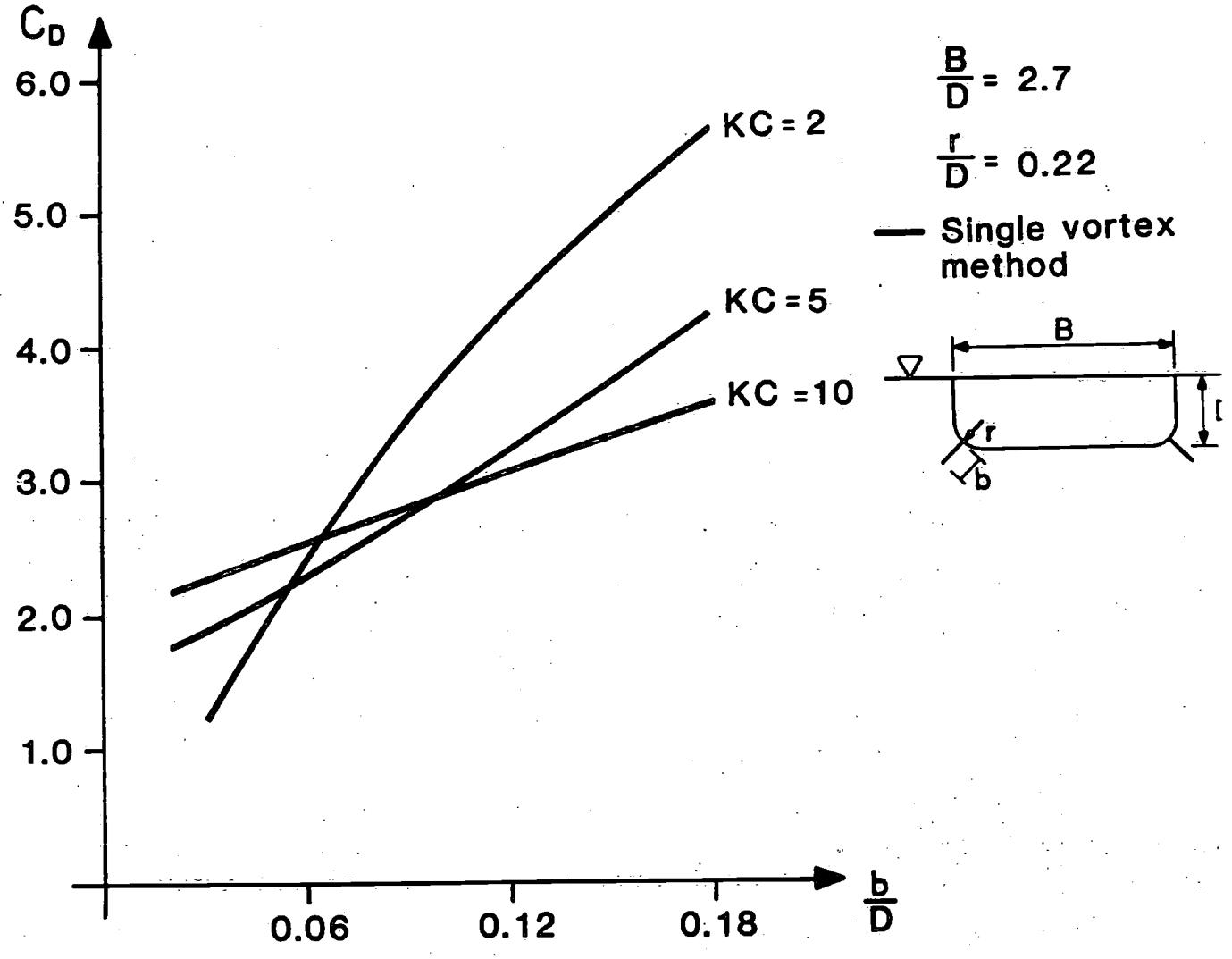
C_D
6.0
5.0
4.0
3.0
2.0
1.0
KC = 2
KC = 5
KC = 10
0.06
0.12
0.18
b/D
B/D = 2.7
r/D = 0.22
Single vortex method
B
r
b

Figure 8

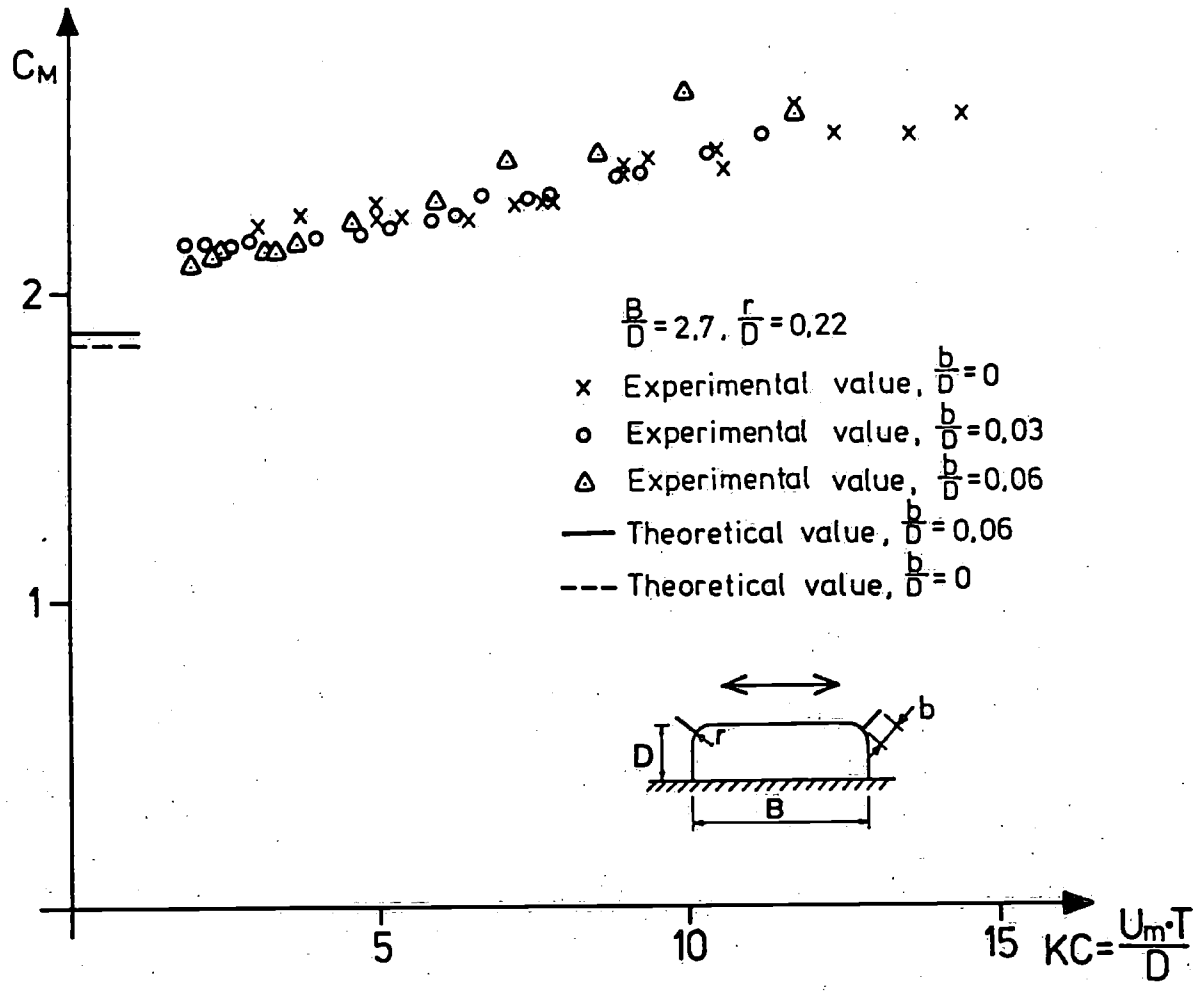
C_M
2
1
5
10
15
KC=$\frac{U_m \cdot T}{D}$
$\frac{B}{D}$ = 2,7 , $\frac{r}{D}$ = 0,22
x Experimental value, $\frac{b}{D}$ = 0
o Experimental value, $\frac{b}{D}$ = 0,03
△ Experimental value, $\frac{b}{D}$ = 0,06
—— Theoretical value, $\frac{b}{D}$ = 0,06
--- Theoretical value, $\frac{b}{D}$ = 0
D
r
b
B

Figure 9

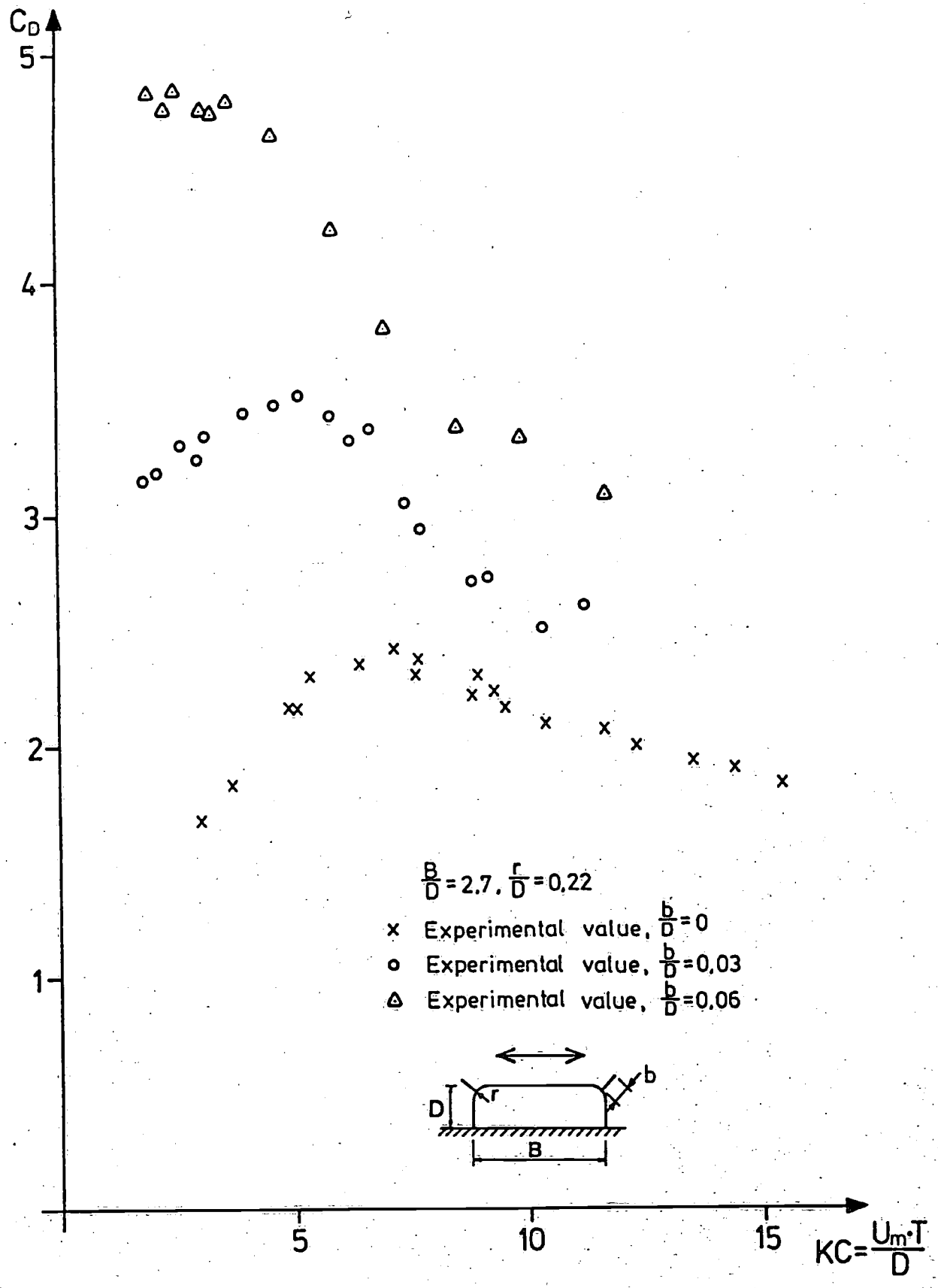
C_D
5
4
3
2
1
5
10
15
$KC=\frac{U_m \cdot T}{D}$
$\frac{B}{D}=2.7,\ \frac{r}{D}=0,22$
Experimental value, $\frac{b}{D}=0$
Experimental value, $\frac{b}{D}=0,03$
Experimental value, $\frac{b}{D}=0,06$
D
r
b
B

Figure 10

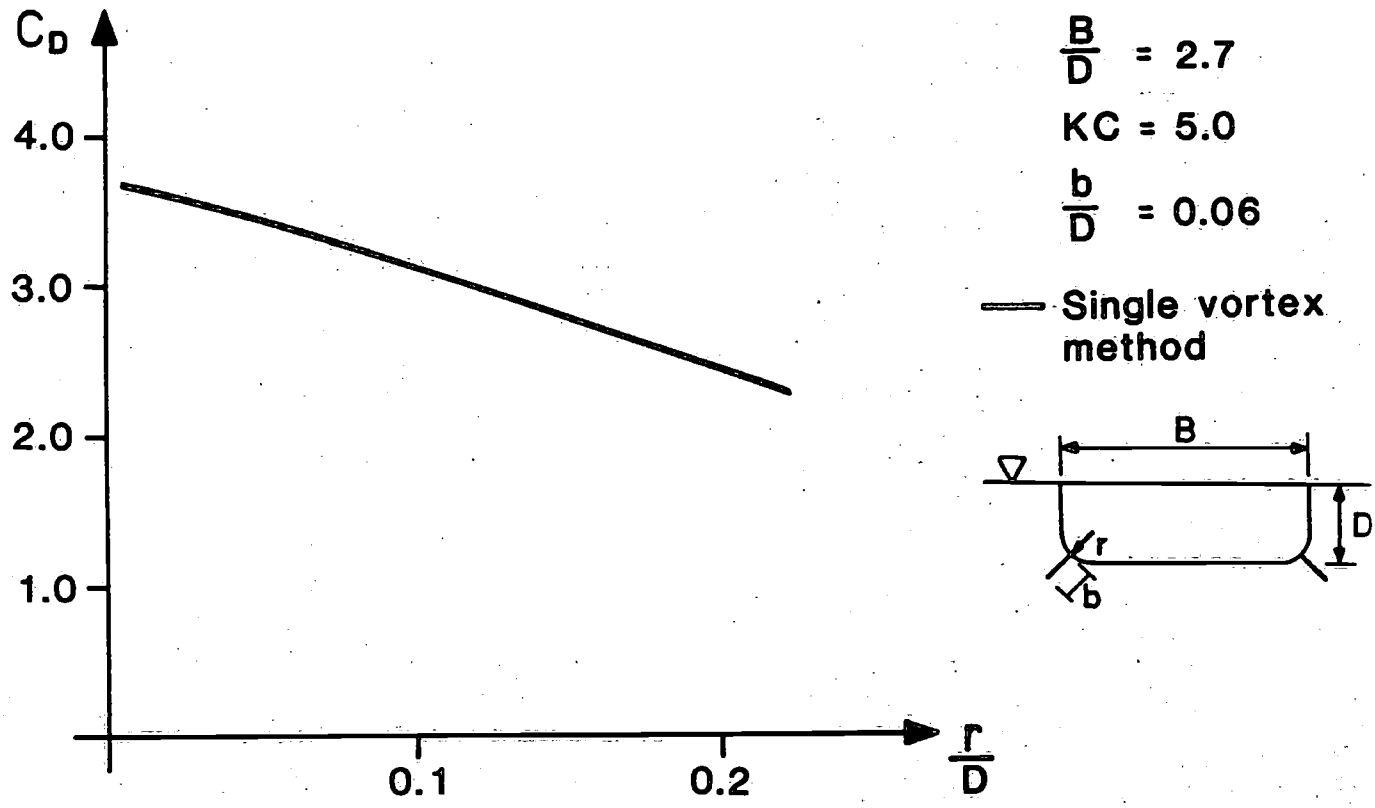
C_D
4.0
3.0
2.0
1.0
0.1
0.2
$\frac{r}{D}$
$\frac{B}{D}$ = 2.7
KC = 5.0
$\frac{b}{D}$ = 0.06
Single vortex method
B
D
r
b

Figure 11

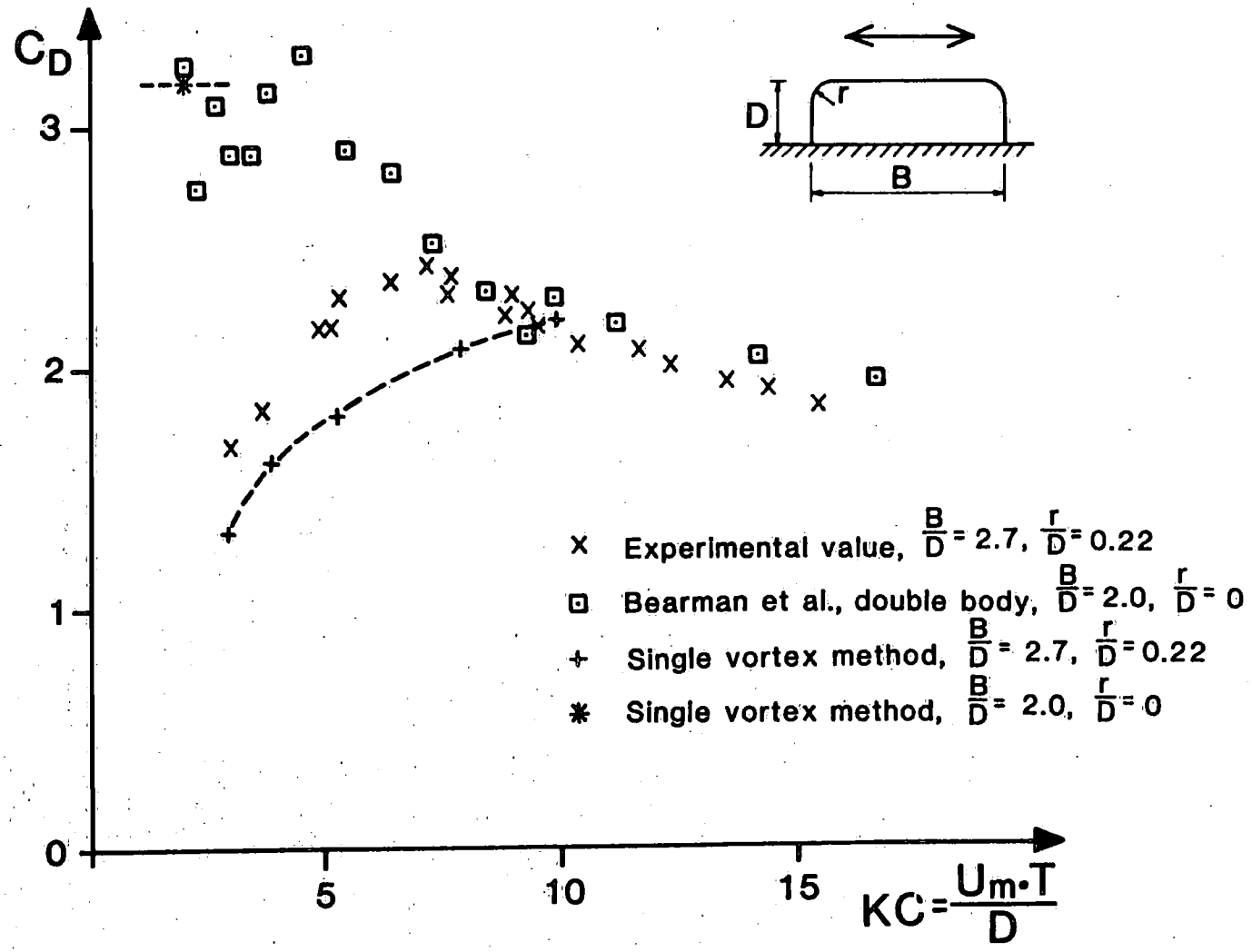
C_D
3
2
1
0
5
10
15
$KC = \frac{U_m \cdot T}{D}$
D
r
B
× Experimental value, $\frac{B}{D} = 2.7$, $\frac{r}{D} = 0.22$
⊡ Bearman et al., double body, $\frac{B}{D} = 2.0$, $\frac{r}{D} = 0$
+ Single vortex method, $\frac{B}{D} = 2.7$, $\frac{r}{D} = 0.22$
✱ Single vortex method, $\frac{B}{D} = 2.0$, $\frac{r}{D} = 0$

Figure 12

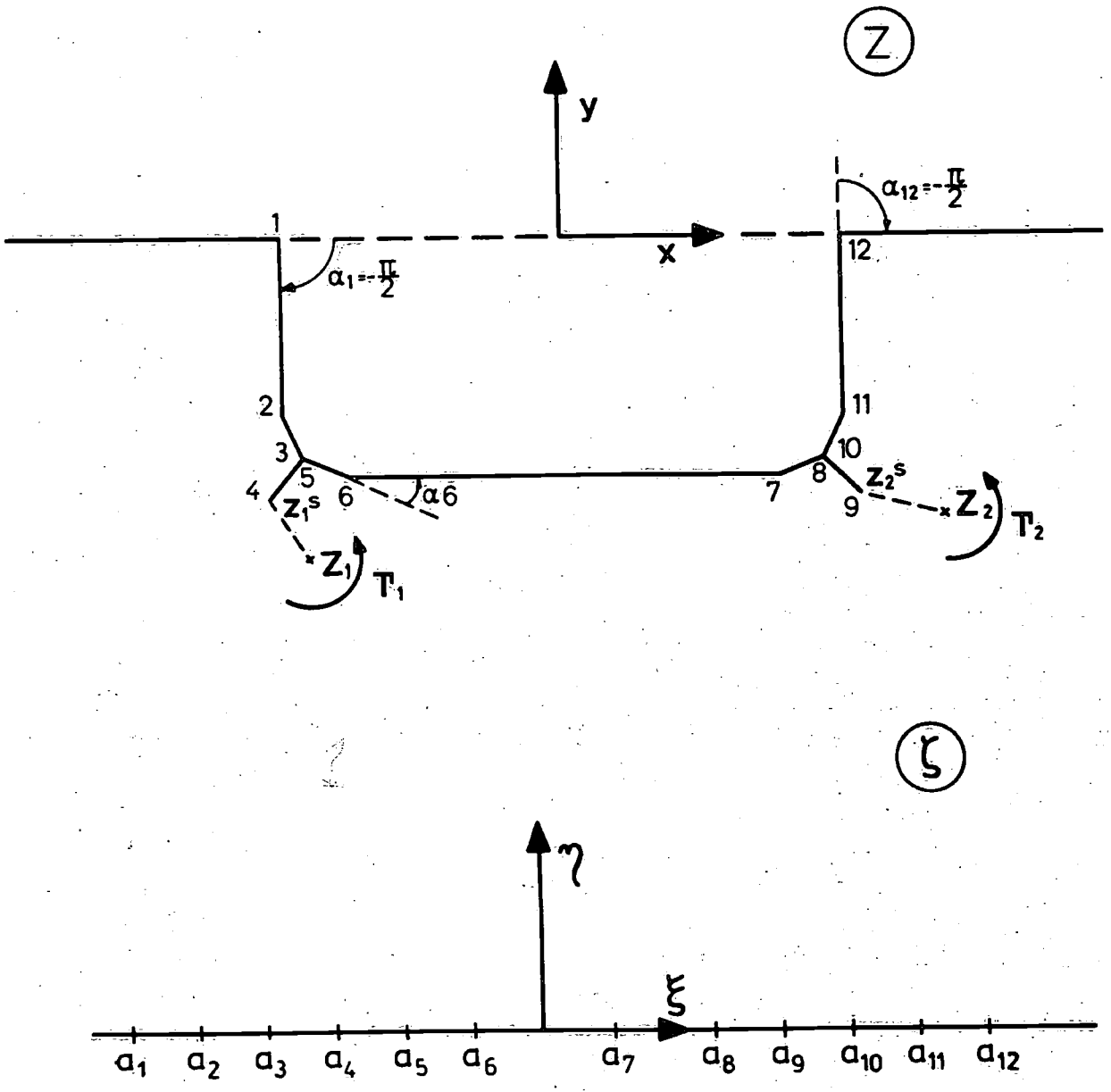
Z
y
x
1
12
$\alpha_1 = -\frac{\pi}{2}$
$\alpha_{12} = -\frac{\pi}{2}$
2
3
4
5
6
7
8
9
10
11
α_6
z_1^s
z_1
T_1
z_2^s
z_2
T_2
ζ
η
ξ
a_1
a_2
a_3
a_4
a_5
a_6
a_7
a_8
a_9
a_{10}
a_{11}
a_{12}

Figure 13

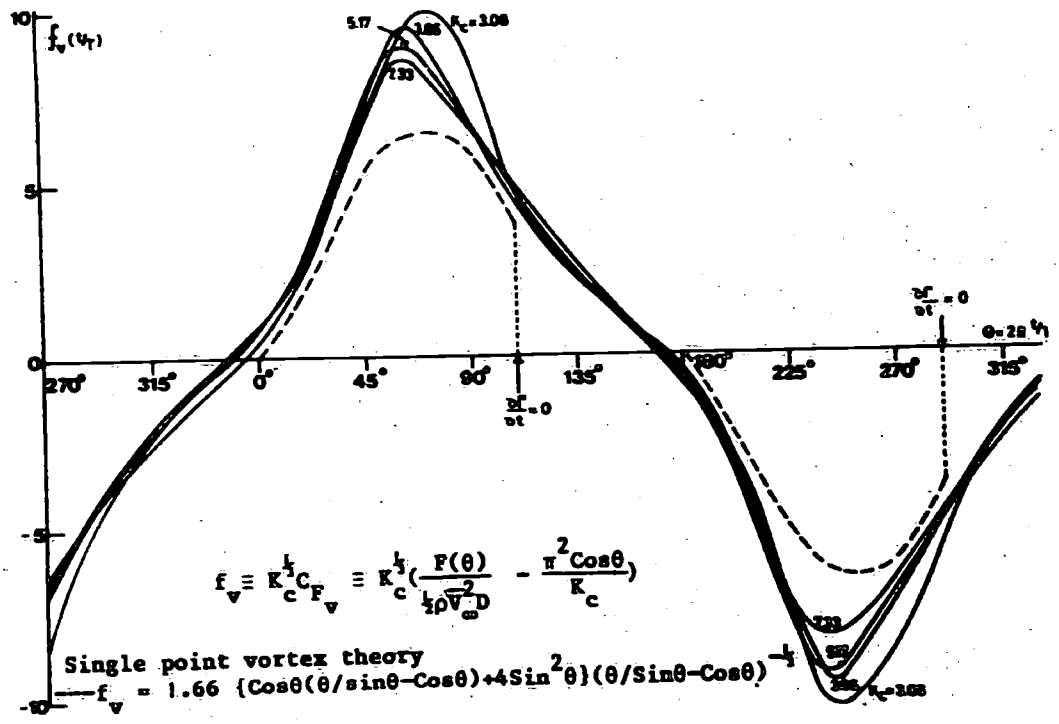
10
5
0
-5
-10
5.17
3.66
2.99
$K_c = 3.08$
270°
315°
0°
45°
90°
135°
180°
225°
270°
315°
$\frac{\partial \Gamma}{\partial t} = 0$
$\theta = 2\pi$
$f_v \equiv K_c^{\frac{1}{3}} C_{F_v} \equiv K_c^{\frac{1}{3}} \left(\frac{F(\theta)}{\frac{1}{2}\rho \bar{V}_\infty^2 D} - \frac{\pi^2 \cos\theta}{K_c} \right)$
Single point vortex theory
$f_v = 1.66 \{\cos\theta(\theta/\sin\theta - \cos\theta) + 4\sin^2\theta\}(\theta/\sin\theta - \cos\theta)^{-\frac{1}{3}}$

Figure 14

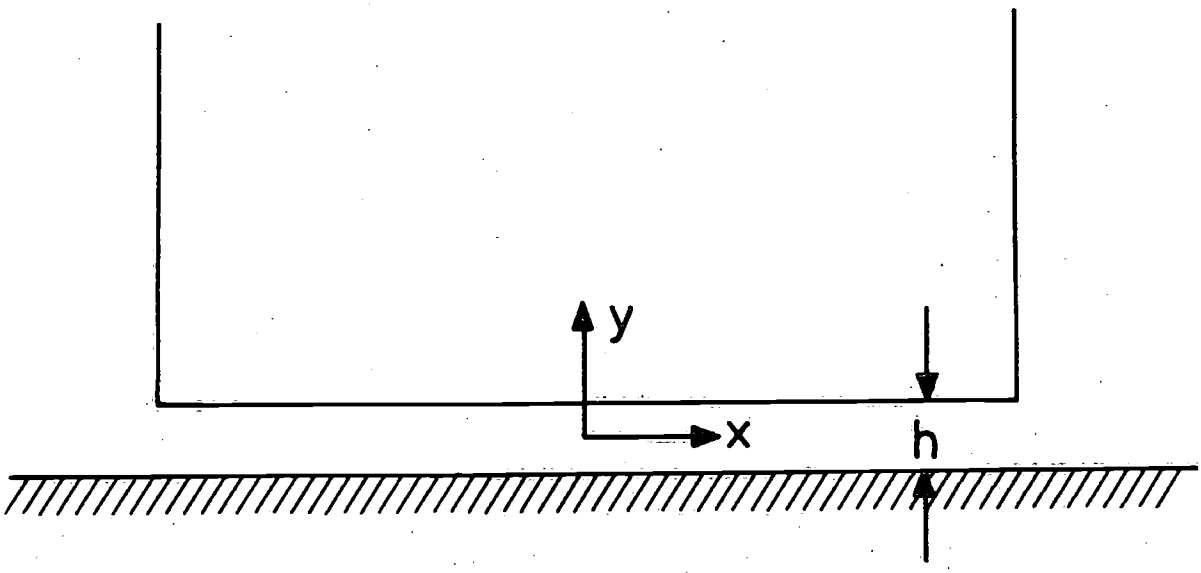

Figure 15

Midship section with finite bilge radius.

$\frac{B}{D} = 2.7$ $\frac{r}{D} = 0.22$

KC	4	5.4	10.8
$C_D(\beta=\frac{\pi}{4})$	1.6	1.8	2.2
$C_D(\beta=\frac{\pi}{8})$	1.25	1.35	1.6

Table 1. Influence of separation point